ICCV
#572

ICCV
#572

ICCV 2017 Submission #572. CONFIDENTIAL REVIEW COPY. DO NOT DISTRIBUTE.

Multi-channel Weighted Nuclear Norm Minimization for Real Color Image Denoising

Anonymous ICCV submission

Paper ID 572

Abstract

The noise structures among the R, G, B channels of real images are quite different due to the preprocessing steps in digital camera pipelines. This makes the real image denoising problem much more complex than traditional grayscale image denoising. In this paper, we propose a multi-channel optimization model for real color image denoising. Specifically, we introduce a weighting matrix into the data term to process adaptively each part of R, G, B channels in the joint patches concatenated by corresponding patches in these channels. In the regularization term, we employ the weighted nuclear norm to exploit the non-local self similar property. The proposed multi-channel weighted nuclear norm minimization (MC-WNNM) model is much more complex than the standard WNNM model. To solve this new problem, we reformulate the MC-WNNM model into a linear equality-constrained problem and solve it under the alternating direction method of multipliers (ADMM) framework. Each alternative updating step has closed-form solution and the convergence results are given. Experiments on benchmark datasets demonstrate that the proposed model outperforms state-of-the-art denoising methods on synthetic as well as real-world noisy images.

1. Introduction

Image denoising is an important problem in enhancing the image quality in computer vision systems. The traditional grayscale image denoising problem aims to recover the clean image $\mathbf{x}$ from the noisy observation $\mathbf{y} = \mathbf{x} + \mathbf{n}$, where $\mathbf{n}$ is often assumed to be additive white Gaussian noise (AWGN). Most image denoising methods in this field either employ the non-local self similarity (NSS) of natural images [1–7] or learn generative or discriminative denoisers from paired natural clean images and synthetic noisy images [8–12]. Among these methods, the weighted nuclear norm minimization (WNNM) method achieves excellent denoising performance by exploiting the NSS property

via low rank regularization.

The real color image denoising problem is not a trivial extension from single channel (grayscale image) to multiple channels (color image). The reason is that the noise in standard RGB (sRGB) space, though could be modeled as AWGN, are with different variances for different channels [13] due to the on-board processing steps in digital camera pipelines [14, 15]. This makes the real color image denoising problem much more complex. Directly applying the denoising methods [1–12] for grayscale images to each channel of color images separately would obtain bad performance [16]. There are several work [14, 16–20] proposed specifically for color image denoising. The method [17] first transforms the color images into the luminance/chrominance space such as YCbCr before denoising, but this would make the noise distribution more complex in color images. The methods of [16, 20] process the joint patches concatenated by the corresponding patches in R, G, B channels and treat equally the patches in different channels. This would generate false colors or artifacts [16]. The methods of [14, 18, 19] ignore the non-local self similarity property of natural images, and their performance would be largely depressed [2, 7].

In order to deal with the R, G, B channels in color images more effectively, different noise properties of different channels should be considered in solving real color image denoising problem. Besides, due to its expressive denoising performance, the WNNM model [7] is employed to exploit the NSS property of natural images. In this paper, we proposed a multi-channel WNNM (MC-WNNM) model for real color image denoising. By introducing a weighting matrix to the WNNM model, the proposed MC-WNNM model no longer has closed-form solutions and is more challenging to solve. By reformulating the proposed MC-WNNM model into a linear equality-constrained program with two variables, the relaxed problem can be solved under the alternating direction method of multipliers (ADMM) [21] framework. Each variable can be updated with closed-form solution [7, 22]. We also give the convergence results with detailed proof to guarantee a rational termination of the pro-

ICCV
#572

ICCV
#572

ICCV 2017 Submission #572. CONFIDENTIAL REVIEW COPY. DO NOT DISTRIBUTE.

posed algorithm.

2. Related Work

2.1. Weighted Nuclear Norm Minimization

As an extension to the nuclear norm minimization (NNM) model [23], the weighted nuclear norm minimization (WNNM) model [7] is described as

$$\min_{\mathbf{X}} \|\mathbf{Y} - \mathbf{X}\|_F^2 + \|\mathbf{X}\|_{\boldsymbol{w},*}, \qquad (1)$$

where $\|\mathbf{X}\|_{\boldsymbol{w},*} = \sum_i w_i \sigma_i(\mathbf{X})$ is the weighted nuclear norm of matrix $\mathbf{X}$, and $\boldsymbol{w} = [w_1, ..., w_n]^\top, w_i \geq 0$ is the weight vector, $\sigma_i(\mathbf{X})$ is the i-th singular value of matrix $\mathbf{X}$. According to the Corollary 1 of [24], if the weights are non-decreasing, the problem (1) has closed-form solution:

$$\hat{\mathbf{X}} = \mathbf{U} \mathcal{S}_{\boldsymbol{w}/2}(\boldsymbol{\Sigma}) \mathbf{V}^\top, \qquad (2)$$

where $\mathbf{Y} = \mathbf{U}\boldsymbol{\Sigma}\mathbf{V}^\top$ is the singular value decomposition [25] of $\mathbf{Y}$ and $\mathcal{S}_\tau(\bullet)$ is the generalized soft-thresholding operator with weight vector $\boldsymbol{w}$:

$$\mathcal{S}_{\boldsymbol{w}/2}(\boldsymbol{\Sigma}_{ii}) = \max(\boldsymbol{\Sigma}_{ii} - w_{ii}/2, 0). \qquad (3)$$

Though having achieved excellent performance on grayscale image denoising, the WNNM model would generate false colors or artifacts [16], if being directly extended to real color image denoising by processing each channel separately or joint vectors concatenated by multiple channels. In this paper, for real noisy image denoising, we propose a multi-channel WNNM model which preserve the power of WNNM and be able to process the differences among different channels.

2.2. Real Color Image Denoising

During the last decade, several denoising methods are proposed for real color image denoising [17–20]. Among them, the CBM3D [17] first transform the RGB image into luminance-chrominance space (e.g., YCbCr) and then apply the famous BM3D method [2] on each channel separately with the patches being grouped only in the luminance channel. In [18], the authors proposed the "Noise Level Function" to estimate and remove the noise for each channel in natural images. However, the methods processing each channel separately would achieve inferior performance than processing jointly these channels [16]. The methods of [19, 20, 26] perform real color image denoising by concatenating the patches in R, G, B channels into joint vectors. However, the concatenation would treat each channel equally and ignore the different noise properties among these channels. The method in [14] models the cross-channel noise in real noisy image as a multivariate Gaussian and the noise is removed by the Bayesian nonlocal means filter [27]. The commercial software Neat Image [28] estimates the noise parameters from a flat region of the

given noisy image and filters the noise correspondingly. But these methods [14, 28] ignore the non-local self similarity property of natural images [2, 7].

In this paper, we introduce a weighting matrix which add different weights to different channels for color image denoising. The proposed multi-channel method can effectively solve the problem of different noise structures among different channels.

3. Color Image Denoising via Multi-channel Weighted Nuclear Norm Minimization

3.1. The Problem

The color image denoising problem is to recover the clean image $\mathbf{x}_c$ from its noisy version $\mathbf{y}_c = \mathbf{x}_c + \mathbf{n}_c$, where $c = \{r, g, b\}$ is the index of R, G, B channels and $\mathbf{n}_c$ is the noise in c-th channel. Given a noisy color image $\mathbf{y}_c$, each local patch of size $p \times p \times 3$ is extracted and stretched to a patch vector $\mathbf{y} = [\mathbf{y}_r^\top \ \mathbf{y}_g^\top \ \mathbf{y}_b^\top]^\top \in \mathbb{R}^{3p^2}$, where $\mathbf{y}_r, \mathbf{y}_g, \mathbf{y}_b \in \mathbb{R}^{p^2}$ are corresponding patches in R, G, B, channels. For each local patch $\mathbf{y}$, we search the M most similar patches to it (including $\mathbf{y}$ itself) by Euclidean distance in a $W \times W$ local region around it. We stack the M similar patches column by column to form a noisy patch matrix $\mathbf{Y} = \mathbf{X} + \mathbf{N} \in \mathbb{R}^{3p^2 \times M}$, where $\mathbf{X}$ and $\mathbf{N}$ the corresponding clean and noise patch matrices.

According to [13], the noise in standard RGB (sRGB) space, though could be modeled as additive white Gaussian (AWGN), are with different variances for different channels. Therefore, it is problematic to directly apply denoising methods to the joint vectors concatenated by corresponding patches of the R, G, B channels. To validate this point, in Fig. 1, we show the clean image "kodim08" taken from the Kodak PhotoCD dataset (http://r0k.us/graphics/kodak/), its degraded version generated by adding synthetic additive white Gaussian noise (AWGN) to each channel of "kodim08", and the denoised image by applying WNNM [24] on the joint vectors concatenated from R, G, B channels of the degraded image. The standard derivations of AWGN added to the R, G, B channels are $\sigma_r = 40$, $\sigma_g = 20$, $\sigma_b = 30$, respectively. The input standard derivation of the noise for the concatenated WNNM method is set as the Root Mean Square (RMS) of those in each channel, i.e., $\sigma = \sqrt{(\sigma_r^2 + \sigma_g^2 + \sigma_b^2)/3} \approx 31.1$. From Fig. 1, one can see that the concatenated WNNM method treating each channel equally would remain some noise in the R channel, while over-smoothing the G channel of the degraded image. Hence, if the patches of different channels are treated differently on the concatenated patch vectors, the degraded images would be recovered with better visual qualities.

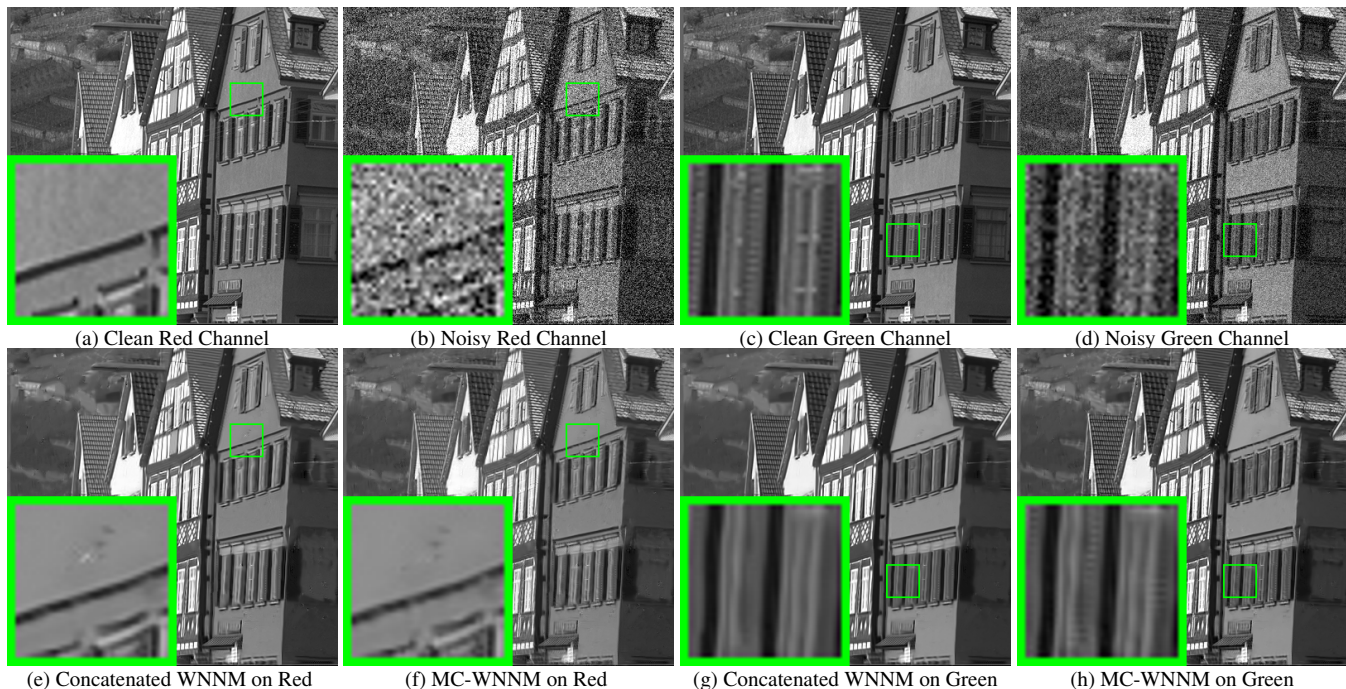In order to process each channel differently while still

ICCV
#572

ICCV
#572

ICCV 2017 Submission #572. CONFIDENTIAL REVIEW COPY. DO NOT DISTRIBUTE.

(a) Clean Red Channel   (b) Noisy Red Channel   (c) Clean Green Channel   (d) Noisy Green Channel

(e) Concatenated WNNM on Red   (f) MC-WNNM on Red   (g) Concatenated WNNM on Green   (h) MC-WNNM on Green

Figure 1. The Red and Green channels of the image "kodim08" from the Kodak PhotoCD dataset, its synthetic noisy version, and the images recovered by the concatenated WNNM and the proposed MC-WNNMW methods.

exploiting the joint structures of the color images, in this paper, we introduce a weighting matrix $\mathbf{W}$ to the concatenated WNNM method and propose a novel multi-channel WNNM (MC-WNNM) model:

$$\min_{\mathbf{X}} \|\mathbf{W}(\mathbf{Y} - \mathbf{X})\|_F^2 + \|\mathbf{X}\|_{\boldsymbol{w},*}. \quad (4)$$

In [24] and this paper, the weight vector $\boldsymbol{w}$ is set as $w_i = \frac{C}{|\sigma_i(\mathbf{X})| + \epsilon}$ where $\epsilon > 0$ is a small number to avoid zero numerator. Please refer to [24] for more details about $\boldsymbol{w}$. Note that if $\sigma_r = \sigma_g = \sigma_b$, the proposed MC-WNNM model will be reduced to the concatenated WNNM model as a special case. The setting of the weighting matrix $\mathbf{W}$ and the solution of the proposed MC-WNNM model will be introduced in the next subsections.

3.2. The Setting of Weighting Matrix $\mathbf{W}$

Assume the noisy patch matrix $\mathbf{Y} = [\mathbf{Y}_r^\top \ \mathbf{Y}_g^\top \ \mathbf{Y}_b^\top]^\top$, where $\mathbf{Y}_r, \mathbf{Y}_g, \mathbf{Y}_b$ are matrices of similar patches in R, G, B channels, respectively. The corresponding clean matrix $\mathbf{X} = [\mathbf{X}_r^\top \ \mathbf{X}_g^\top \ \mathbf{X}_b^\top]^\top$, where $\mathbf{X}_r, \mathbf{X}_g, \mathbf{X}_b$ are similarly defined. For simplicity, in this paper, we assume the noise are independent among the R, G, B channels and i.i.d. in each channel. Therefore, the weighting matrix $\mathbf{W}$ is diagonal and can be determined under the Bayesian framework:

$$\hat{\mathbf{X}} = \arg\max_{\mathbf{X}} \ln P(\mathbf{X}|\mathbf{Y}, \boldsymbol{w})$$
$$= \arg\max_{\mathbf{X}} \{\ln P(\mathbf{Y}|\mathbf{X}) + \ln P(\mathbf{X}|\boldsymbol{w})\}. \quad (5)$$

The log-likelihood term $\ln P(\mathbf{Y}|\mathbf{X})$ is characterized by the statistics of noise, which is assumed to be channel-wise independent white Gaussian with standard deviations $\{\sigma_r, \sigma_g, \sigma_b\}$. So we have

$$P(\mathbf{Y}|\mathbf{X}) = \prod_{c \in \{r,g,b\}} (2\pi\sigma_c^2)^{-\frac{3p^2}{2}} \exp(-\frac{1}{2\sigma_c^2}\|\mathbf{Y}_c - \mathbf{X}_c\|_F^2). \quad (6)$$

We assume that the matrix $\mathbf{X}$ follows the following distribution

$$P(\mathbf{X}|\boldsymbol{w}) \propto \exp(-\frac{1}{2}\|\mathbf{X}\|_{\boldsymbol{w},*}). \quad (7)$$

Putting (7) and (6) into (5), we have

$$\hat{\mathbf{X}} = \arg\min_{\mathbf{X}} \sum_{c \in \{r,g,b\}} \frac{1}{\sigma_c^2}\|(\mathbf{Y}_c - \mathbf{X}_c)\|_F^2 + \|\mathbf{X}\|_{\boldsymbol{w},*} \quad (8)$$
$$= \arg\min_{\mathbf{X}} \|\mathbf{W}(\mathbf{Y} - \mathbf{X})\|_F^2 + \|\mathbf{X}\|_{\boldsymbol{w},*},$$

where

$$\mathbf{W} = \begin{pmatrix} \sigma_r^{-1}\mathbf{I} & \mathbf{0} & \mathbf{0} \\ \mathbf{0} & \sigma_g^{-1}\mathbf{I} & \mathbf{0} \\ \mathbf{0} & \mathbf{0} & \sigma_b^{-1}\mathbf{I} \end{pmatrix}. \quad (9)$$

where $\mathbf{I} \in \mathbb{R}^{p^2 \times p^2}$ is the identity matrix. Hence, the weighting matrix $\mathbf{W}$ is determined to contribute equal weights for the pixel values in the same channel, while different weights for those in different channels. The experimental (which will be introduced later) results have already demonstrated that this form of weighting matrix have already generated the best denoising performance on synthetic and real noisy images in benchmark datasets.

3

ICCV
#572

ICCV 2017 Submission #572. CONFIDENTIAL REVIEW COPY. DO NOT DISTRIBUTE.

ICCV
#572

3.3. Optimization

The proposed MC-WNNM model could not be solved in an analytical form while the original WNNM model [24] could. In the WNNM model, when the weights on singular values are non-descending, the weighted nuclear norm proximal operator [24] can have global optimum with closed-form solution. However, such property is not valid for the proposed MC-WNNM model. The reason is that the weighting matrix $\mathbf{W}$ is applied to the rows of matrix $\mathbf{X}$ instead of its singular values. Besides, the elements in $\mathbf{W}$ is not in a non-descending order with respect to the singular values of $\mathbf{X}$. This makes the proposed model more difficult to solve when compared to the original WNNM model [24].

By introducing an augmented variable $\mathbf{Z}$, the MC-WNNM model is reformulated as a linear equality-constrained problem with two variables $\mathbf{X}$ and $\mathbf{Z}$:

$$\min_{\mathbf{X}, \mathbf{Z}} \|\mathbf{W}(\mathbf{Y} - \mathbf{X})\|_F^2 + \|\mathbf{Z}\|_{\boldsymbol{w}, *} \quad \text{s.t.} \quad \mathbf{X} = \mathbf{Z}. \quad (10)$$

Since the objective function is separable across the two variables, the problem (10) can be solved under the alternating direction method of multipliers (ADMM) [21] framework. We can derive its augmented Lagrangian function as:

$$\mathcal{L}(\mathbf{X}, \mathbf{Z}, \mathbf{A}, \rho) = \|\mathbf{W}(\mathbf{Y} - \mathbf{X})\|_F^2 + \|\mathbf{Z}\|_{\boldsymbol{w}, *}$$
$$+ \langle \mathbf{A}, \mathbf{X} - \mathbf{Z} \rangle + \frac{\rho}{2} \|\mathbf{X} - \mathbf{Z}\|_F^2, \quad (11)$$

where $\mathbf{A}$ is the augmented Lagrangian multiplier and $\rho > 0$ is the penalty parameter. We initialize the matrix variables $\mathbf{X}_0$, $\mathbf{Z}_0$, and $\mathbf{A}_0$ to be zero matrix of suitable size and $\rho_0 > 0$ to be a suitable value. Denote by $(\mathbf{X}_k, \mathbf{Z}_k)$ and $\mathbf{A}_k$ the optimization variables and Lagrange multiplier at iteration k ($k = 0, 1, 2, ...$), respectively. By taking derivative of the Lagrangian function $\mathcal{L}$ with respect to the variables $\mathbf{X}$ and $\mathbf{Z}$ and setting the derivative function to be zero, we can alternatively update the ADMM algorithm iteratively as follows:

(1) **Update X while fixing Z and A**:

$$\mathbf{X}_{k+1} = \arg\min_{\mathbf{X}} \|\mathbf{W}(\mathbf{Y} - \mathbf{X})\|_F^2 + \frac{\rho_k}{2} \|\mathbf{X} - \mathbf{Z}_k + \rho_k^{-1}\mathbf{A}_k\|_F^2. \quad (12)$$

This is a standard least squares regression problem with closed-form solution:

$$\mathbf{X}_{k+1} = (\mathbf{W}^\top\mathbf{W} + \frac{\rho_k}{2}\mathbf{I})^{-1}(\mathbf{W}^\top\mathbf{W}\mathbf{Y} + \frac{\rho_k}{2}\mathbf{Z}_k - \frac{1}{2}\mathbf{A}_k). \quad (13)$$

(2) **Update Z while fixing X and A**:

$$\mathbf{Z}_{k+1} = \arg\min_{\mathbf{Z}} \frac{\rho_k}{2} \|\mathbf{Z} - (\mathbf{X}_{k+1} + \rho_k^{-1}\mathbf{A}_k)\|_F^2 + \|\mathbf{Z}\|_{\boldsymbol{w}, *}. \quad (14)$$

According to the Theorem 1 in [24], given the $\mathbf{X}_{k+1} + \rho_k^{-1}\mathbf{A}_k = \mathbf{U}_k\boldsymbol{\Sigma}_k\mathbf{V}_k^\top$ be the SVD of $\mathbf{X}_{k+1} + \rho_k^{-1}\mathbf{A}_k$, where $\boldsymbol{\Sigma}_k = \begin{pmatrix} \text{diag}(\sigma_1, \sigma_2, ..., \sigma_n) \\ \mathbf{0} \end{pmatrix} \in \mathbb{R}^{m \times n}$, then the

---

Algorithm 1: Solve MC-WNNM via ADMM
Input: Matrices $\mathbf{Y}$ and $\mathbf{W}$, $\mu > 1$, Tol > 0, K_1;
Initialization: $\mathbf{X}_0 = \mathbf{Z}_0 = \mathbf{A}_0 = \mathbf{0}$, $\rho_0 > 0$, T = False, $\quad k = 0$;
While (T == false) **do**
1. Update $\mathbf{X}_{k+1}$ as
$\mathbf{X}_{k+1} = (\mathbf{W}^\top\mathbf{W} + \frac{\rho_k}{2}\mathbf{I})^{-1}(\mathbf{W}^\top\mathbf{W}\mathbf{Y} + \frac{\rho_k}{2}\mathbf{Z}_k - \frac{1}{2}\mathbf{A}_k)$
2. Update $\mathbf{Z}_{k+1}$ by solving the problem
$\quad \min_{\mathbf{Z}} \frac{\rho_k}{2}\|\mathbf{Z} - (\mathbf{X}_{k+1} + \rho_k^{-1}\mathbf{A}_k)\|_F^2 + \|\mathbf{Z}\|_{\boldsymbol{w},*}$
3. Update $\mathbf{A}_{k+1}$ as $\mathbf{A}_{k+1} = \mathbf{A}_k + \rho_k(\mathbf{X}_{k+1} - \mathbf{Z}_{k+1})$
4. Update $\rho_{k+1} = \mu * \rho_k$;
5. $k \leftarrow k + 1$;
if (Convergence condition is satisfied) or ($k \geq K_1$)
5.   T $\leftarrow$ True
end if
end while
Output: Matrices $\mathbf{X}$ and $\mathbf{Z}$.

global optimum of the problem (14) is $\hat{\mathbf{Z}} = \mathbf{U}_k\hat{\boldsymbol{\Sigma}}_k\mathbf{V}_k^\top$, where $\hat{\boldsymbol{\Sigma}}_k = \begin{pmatrix} \text{diag}(\hat{\sigma}_1, \hat{\sigma}_2, ..., \hat{\sigma}_n) \\ \mathbf{0} \end{pmatrix} \in \mathbb{R}^{m \times n}$ and $(\hat{\sigma}_1, \hat{\sigma}_2, ..., \hat{\sigma}_n)$ is the solution to the following convex optimization problem:

$$\min_{\hat{\sigma}_1, \hat{\sigma}_2, ..., \hat{\sigma}_n} \sum_{i=1}^n (\sigma_i - \hat{\sigma}_i)^2 + \frac{2w_i}{\rho_k}\hat{\sigma}_i \quad (15)$$
$$\text{s.t.} \quad \hat{\sigma}_1 \geq \hat{\sigma}_2 \geq ... \geq \hat{\sigma}_n \geq 0.$$

According to the Remark 1 in [24], the problem above has closed-form solution

$$\hat{\sigma}_i = \begin{cases} 0 & \text{if } c_2 < 0 \\ \frac{c_1 + \sqrt{c_2}}{2} & \text{if } c_2 \geq 0 \end{cases}, \quad (16)$$

where $c_1 = \sigma_i - \epsilon$, $c_2 = (\sigma_i - \epsilon)^2 - \frac{8C}{\rho_k}$, $\epsilon > 0$ is a small number, and C is set as $\sqrt{2M}$ by experience in [24].

(3) **Update A while fixing X and Z**:

$$\mathbf{A}_{k+1} = \mathbf{A}_k + \rho_k(\mathbf{X}_{k+1} - \mathbf{Z}_{k+1}). \quad (17)$$

(4) **Update ρ_k**: $\rho_{k+1} = \mu * \rho_k$, where $\mu > 1$.

The above alternative updating steps are repeated until the convergence condition is satisfied or the number of iterations exceeds a preset maximum number, e.g., K_1. The convergence condition of the ADMM algorithm is: $\|\mathbf{X}_{k+1} - \mathbf{Z}_{k+1}\|_F \leq$ Tol, $\|\mathbf{X}_{k+1} - \mathbf{X}_k\|_F \leq$ Tol, and $\|\mathbf{Z}_{k+1} - \mathbf{Z}_k\|_F \leq$ Tol are simultaneously satisfied, where Tol > 0 is a small tolerance. We summarize the updating steps in Algorithm 1. The convergence analysis of the proposed Algorithm 1 is given in Theorem 1. Note that since the weighted nuclear norm is non-convex in general, we employ an unbounded sequence of $\{\rho_k\}$ here to make sure that the Algorithm 1 is convergent.

ICCV
#572

ICCV
#572

ICCV 2017 Submission #572. CONFIDENTIAL REVIEW COPY. DO NOT DISTRIBUTE.

Theorem 1. *Assume the weights in $\mathbf{w}$ are in a non-descending order, the sequence $\{\mathbf{X}_k\}$, $\{\mathbf{Z}_k\}$, and $\{\mathbf{A}_k\}$ generated in Algorithm 1 satisfy:*

$$(a) \lim_{k\to\infty} \|\mathbf{X}_{k+1} - \mathbf{Z}_{k+1}\|_F = 0; \qquad (18)$$

$$(b) \lim_{k\to\infty} \|\mathbf{X}_{k+1} - \mathbf{X}_k\|_F = 0; \qquad (19)$$

$$(c) \lim_{k\to\infty} \|\mathbf{Z}_{k+1} - \mathbf{Z}_k\|_F = 0. \qquad (20)$$

Proof. We give proof sketch here and detailed proof of this theorem can be found in supplementary files. We can first proof that the sequence $\{\mathbf{A}_k\}$ generated by Algorithm 1 is upper bounded. Since $\{\rho_k\}$ is unbounded, that is $\lim_{k\to\infty}\rho_k = +\infty$, we can proof that the sequence of Lagrangian function $\{\mathcal{L}(\mathbf{X}_{k+1}, \mathbf{Z}_{k+1}, \mathbf{A}_k, \rho_k)\}$ is also upper bounded. Hence, both $\{\mathbf{W}(\mathbf{Y} - \mathbf{X}_k)\}$ and $\{\mathbf{Z}_k\}$ are upper bounded. According to Eq. (17), we can proof that $\lim_{k\to\infty}\|\mathbf{X}_{k+1} - \mathbf{Z}_{k+1}\|_F = \lim_{k\to\infty}\rho_k^{-1}\|\mathbf{A}_{k+1} - \mathbf{A}_k\|_F = 0$, and (a) is proofed. Then we can proof that $\lim_{k\to\infty}\|\mathbf{X}_{k+1} - \mathbf{X}_k\|_F \leq \lim_{k\to\infty}\|(\mathbf{W}^\top\mathbf{W} + \frac{\rho_k}{2}\mathbf{I})^{-1}(\mathbf{W}^\top\mathbf{W}\mathbf{Y} - \mathbf{W}^\top\mathbf{W}\mathbf{Z}_k - \frac{1}{2}\mathbf{A}_k)\|_F + \rho_k^{-1}\|\mathbf{A}_k - \mathbf{A}_{k-1}\|_F = 0$ and hence (b) is proofed. Then (c) can be proofed by checking that $\lim_{k\to\infty}\|\mathbf{Z}_{k+1} - \mathbf{Z}_k\| \leq \lim_{k\to\infty}\|\mathbf{\Sigma}_{k-1} - \mathcal{S}_{\mathbf{w}/\rho_{k-1}}(\mathbf{\Sigma}_{k-1})\|_F + \|\mathbf{X}_{k+1} - \mathbf{X}_k\|_F + \rho_k^{-1}\|\mathbf{A}_{k-1} + \mathbf{A}_{k+1} - \mathbf{A}_k\|_F = 0$, where $\mathbf{U}_{k-1}\mathbf{\Sigma}_{k-1}\mathbf{V}_{k-1}^\top$ is the SVD of the matrix $\mathbf{X}_k + \rho_{k-1}\mathbf{A}_{k-1}$. $\square$

3.4. The Denoising Algorithm

Given a noisy color image $\mathbf{y}_c$, assume we have extracted N local patches $\{\mathbf{y}_j\}_{j=1}^N$ and corresponding similar patches to form the noisy patch matrices $\{\mathbf{Y}_j\}_{j=1}^N$. The proposed MC-WNNM is applied to the noisy patch matrix $\mathbf{Y}_j$ of each local patch $\mathbf{y}_j$ ($j = 1, ..., N$) of the noisy image $\mathbf{y}_c$. And then all the estimated clean patch matrices $\{\mathbf{X}_j\}_{j=1}^N$ are aggregated together to form the final recovered image $\hat{\mathbf{x}}_c$. To obtain better denoising results, we perform the above denoising procedure for several (K_2) iterations. The proposed MC-WNNM denoising algorithm for color images is summarized in Algorithm 2.

4. Experiments

In this section, we evaluate the proposed MC-WNNM method on synthetic and real noisy image denoising tasks. We compare the proposed method with other state-of-the-art denoising methods, including CBM3D [17], MLP [10], WNNM [7], TNRD [12], "Noise Clinic" (NC) [19, 26], and the commercial software Neat Image (NI) [28].

4.1. Implementation Details

In synthetic experiments, the noise levels in R, G ,B channels are assumed to be known as $\sigma_r, \sigma_g, \sigma_b$. In the real cases, the noise levels in R, G, B channels can be estimated

---

Algorithm 2: Color Image Denoising by MC-WNNM

Input: Noisy image $\mathbf{y}_c$, noise levels $\{\sigma_r, \sigma_g, \sigma_b\}$, K_2;
Initialization: $\hat{\mathbf{x}}_c^{(0)} = \mathbf{y}_c$, $\mathbf{y}_c^{(0)} = \mathbf{y}_c$;
for $k = 1 : K_2$ **do**
1. Set $\mathbf{y}_c^{(k)} = \hat{\mathbf{x}}_c^{(k-1)}$;
2. Extract local patches $\{\mathbf{y}_j\}_{j=1}^N$ from $\mathbf{y}_c^{(k)}$;
   for each patch $\mathbf{y}_j$ **do**
3.   Search non-local similar patches $\mathbf{Y}_j$;
4.   Apply the MC-WNNM model (10) to $\mathbf{Y}_j$ and obtain the estimated $\mathbf{X}_j$;
   end for
5. Aggregate $\{\mathbf{X}_j\}_{j=1}^N$ to form the image $\hat{\mathbf{x}}_c^{(k)}$;
end for
Output: Denoised image $\hat{\mathbf{x}}_c^{K_2}$.

---

via noise estimation methods [29, 30]. In this paper, we employ the method of [30] for its state-of-the-art performance. For the CBM3D method [17], the input noise levels are the Root Mean Square (RMS) as

$$\sigma = \sqrt{(\sigma_r^2 + \sigma_g^2 + \sigma_b^2)/3}. \qquad (21)$$

For the methods of MLP [10] and TNRD [12], we retrain the models on grayscale images following their corresponding strategies at different noise levels from $\sigma = 5$ to $\sigma = 75$ with gap of 5. The denoising on color images is performed by processing separately each channel with the model trained at the same (or nearest) noise levels. NC [19, 26] is a blind image denoising method, so we just submit the noisy images (synthetic or real) to [26] and perform denoising using the default parameters. NI [28] is a commercial software suitable for real image denoising, while the code of CC [14] is not released (but its results on the 15 real noisy images in [14] are available by requesting the authors). Hence, we only compare with CC on dataset [14].

In order to take fully comparison with the original WNNM method [24], we extended the WNNM method [24] for color image denoising in three directions: 1) we apply the WNNM method [24] on each channel separately with corresponding noise levels $\sigma_r, \sigma_g, \sigma_b$. We call this method "WNNM0"; 2) we perform denoising on the joint vectors concatenated by corresponding patches in the R, G, B channels, where the input noise level σ is computed by RMS (Eq. (21)). We call this method "WNNM1"; 3) we set the weighting matrix $\mathbf{W}$ in the proposed MC-WNNM model as $\mathbf{W} = \sigma^{-1}\mathbf{I}$. For fair comparison, we tune all these methods set the same parameters for "WNNM2" and the proposed MC-WNNM methods while achieving the best performance of "WNNM2". For fair comparison, we tune the methods of "WNNM0", "WNNM1", "WNNM2", and the proposed MC-WNNM to achieve corresponding best denoising performance (i.e., highest average PSNR results).

ICCV
#572

ICCV 2017 Submission #572. CONFIDENTIAL REVIEW COPY. DO NOT DISTRIBUTE.
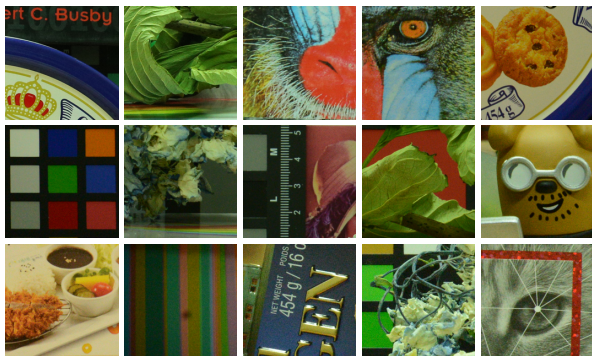
ICCV
#572

Figure 2. The 15 cropped real noisy images used in [14].

4.2. Experiments on Synthetic Color Noisy Images

In this section, we compare the proposed MC-WNNM method with other competing denoising methods [10, 12, 17, 19, 28] as well as the three extended methods ("WNNM0", "WNNM1", and "WNNM2") of the original WNNM method [24] on the 24 high quality color images from the Kodak PhotoCD dataset. The noisy images are generated by adding additive white Gaussian noise (AWGN) with known standard derivations $\sigma_r, \sigma_g, \sigma_b$ for the R, G, B channels, respectively. In this paper, the noise levels we add to each channel of the 24 color images are $\sigma_r = 40, \sigma_g = 20, \sigma_b = 30$, respectively. More experiments can be found in the supplementary files. For the methods of "WNNM2" and MC-WNNM, we set the patch size as $p = 6$, the number of non-local similar patches as $M = 70$, the window size for searching similar patches as $W = 20$, the updating parameter $\mu = 1.001$, the number of iterations in Algorithm 1 as $K_1 = 8$, the number of iterations in Algorithm 2 as $K_2 = 10$. For "WNNM2", the initial penalty parameter is set as $\rho_0 = 10$, while for the proposed MC-WNNM model, the penalty parameter is set as $\rho_0 = 3$.

The PSNR results are listed in Table 1 of the compared methods including CBM3D [17], MLP [10], TNRD [12], NI [28], NC [19, 26], "WNNM0" [24], "WNNM1", "WNNM2" and the proposed MC-WNNM methods. The best PSNR results are highlighted in bold. One can see that on all the 24 images, our method achieves the highest PSNR values over the competing methods. On average PSNR, our proposed method achieves 0.48dB improvements over the "WNNM0" method and outperforms the "WNNM2" by 1.09dB. For space limitation, we leave the visual comparison of the synthetic noisy images denoised by the compared methods in the supplementary files.

4.3. Experiments on Real Color Noisy Images

We evaluate the proposed method on two real noisy image datasets, where the images were captured under indoor or outdoor lighting conditions by different types of cameras and camera settings.

The first dataset is provided in [26], which includes 20 real noisy images collected under uncontrolled outdoor environment. Since there is no "ground truth" of the noisy images, the objective measures such as PSNR cannot be computed on this dataset.

The second dataset is provided in [14], which includes noisy images of 11 static scenes. The noisy images were collected under controlled indoor environment. Each scene was shot 500 times under the same camera and camera setting. The mean image of the 500 shots is roughly taken as the "ground truth", with which the PSNR can be computed. Since the image size is very large (about 7000×5000) and the 11 scenes share repetitive contents, the authors of [14] cropped 15 smaller images (of size 512×512, Fig. 2) to perform experiments. We perform quantitative comparison on the 15 cropped images used in [14]. For each real noisy image, the noise levels in R, G, B channels are estimated by [30]. Since the noise levels are small in real noisy images, for the method of MLP [10] and TNRD [12], we apply the trained models of corresponding methods and choose the best denoising results (highest average PSNR values). Both methods achieves best results when setting the noise levels of the trained models at $\sigma = 10$.

4.3.1 Results on Dataset [26]

Since there is no "ground truth" for the real noisy images in dataset [26], we only compare the visual quality of the denoised images by the compared methods. (Note that method CC [14] is not compared since its code is not available.) Fig. 3 shows the denoised images of "Dog" by the compared methods. It can be seen that CBM3D, MLP, TRND, and "WNNM0" tend to remain some noise caused color artifacts. Besides, "WNNM1" and "WNNM2" tend to oversmooth much the whole image. These results demonstrate that the denoising methods, no matter processing separately or treating equally different channels, are not effective for real noise removal. Though NC and NI methods are specifically developed for real color noisy images, their performance on noise removal is not very satisfactory. In comparison, the proposed MC-WNNM method recovers much better the structures and textures (such as the eye area) than the other competing methods. More visual comparisons on this dataset [26] can be found in the supplementary files.

4.3.2 Results on Dataset [14]

As described in section 4.2, there is a mean image for each noisy image used in dataset [14], and those mean images can be roughly taken as "ground truth" images for quantitative evaluation of denoising algorithms. The PSNR results are listed in Table 2 of the compared methods including CBM3D [17], MLP [10], TNRD [12], NC [19, 26], NI [28], CC [14] (copied from [14]), "WNNM1",

ICCV
#572

ICCV
#572

ICCV 2017 Submission #572. CONFIDENTIAL REVIEW COPY. DO NOT DISTRIBUTE.

Table 1. PSNR(dB) results of different denoising algorithms on 24 natural images.

Image#	CBM3D	MLP	TNRD	NI	NC	WNNM0	WNNM1	WNNM2	MC-WNNM
				$\sigma_r = 40, \sigma_g = 20, \sigma_b = 30$					
1	25.24	25.70	25.74	23.85	24.90	26.01	25.95	25.58	**26.66**
2	28.27	30.12	30.21	25.90	25.87	30.08	30.11	29.80	**30.20**
3	28.81	31.19	31.49	26.00	28.58	31.58	31.61	31.20	**32.25**
4	27.95	29.88	29.86	25.82	25.67	30.13	30.16	29.84	**30.49**
5	25.03	26.00	26.18	24.38	25.15	26.44	26.39	25.32	**26.82**
6	26.24	26.84	26.90	24.65	24.74	27.39	27.30	26.88	**27.98**
7	27.88	30.28	30.40	25.63	27.69	30.47	30.54	29.70	**30.98**
8	25.05	25.59	25.83	24.02	25.30	26.71	26.75	25.26	**26.90**
9	28.44	30.75	30.81	25.94	27.44	30.86	30.92	30.29	**31.49**
10	28.27	30.38	30.57	25.87	28.42	30.65	30.68	29.95	**31.26**
11	26.95	28.00	28.14	25.32	24.67	28.19	28.16	27.61	**28.63**
12	28.76	30.87	31.05	26.01	28.37	30.97	31.06	30.58	**31.48**
13	23.76	23.95	23.99	23.53	22.76	24.27	24.15	23.52	**24.89**
14	26.02	26.97	27.11	24.94	25.68	27.20	27.15	26.55	**27.57**
15	28.38	30.15	30.44	26.06	28.21	30.52	30.60	30.13	**30.81**
16	27.75	28.82	28.87	25.69	26.66	29.27	29.21	29.02	**29.96**
17	27.90	29.57	29.80	25.85	28.32	29.78	29.79	29.16	**30.40**
18	25.77	26.40	26.41	24.74	25.70	26.63	26.56	26.01	**27.22**
19	27.30	28.67	28.81	25.40	26.52	29.19	29.22	28.67	**29.57**
20	28.96	30.40	30.76	24.95	25.90	30.79	30.83	29.97	**31.07**
21	26.54	27.53	27.60	25.06	26.48	27.80	27.75	27.12	**28.34**
22	27.05	28.17	28.27	25.36	26.60	28.21	28.16	27.81	**28.64**
23	29.14	32.31	32.51	26.13	23.24	31.89	31.97	31.21	**32.34**
24	25.75	26.41	26.53	24.55	25.73	27.10	27.03	26.18	**27.59**
Average	27.13	28.54	28.68	25.24	26.19	28.84	28.83	28.22	**29.31**

(a) Noisy [26]   (b) CBM3D [17]   (c) MLP [10]   (d) TNRD [12]   (e) NI [28]

(f) NC [19, 26]   (g) WNNM0 [7]   (h) WNNM1 [7]   (i) WNNM2 [7]   (j) MC-WNNM
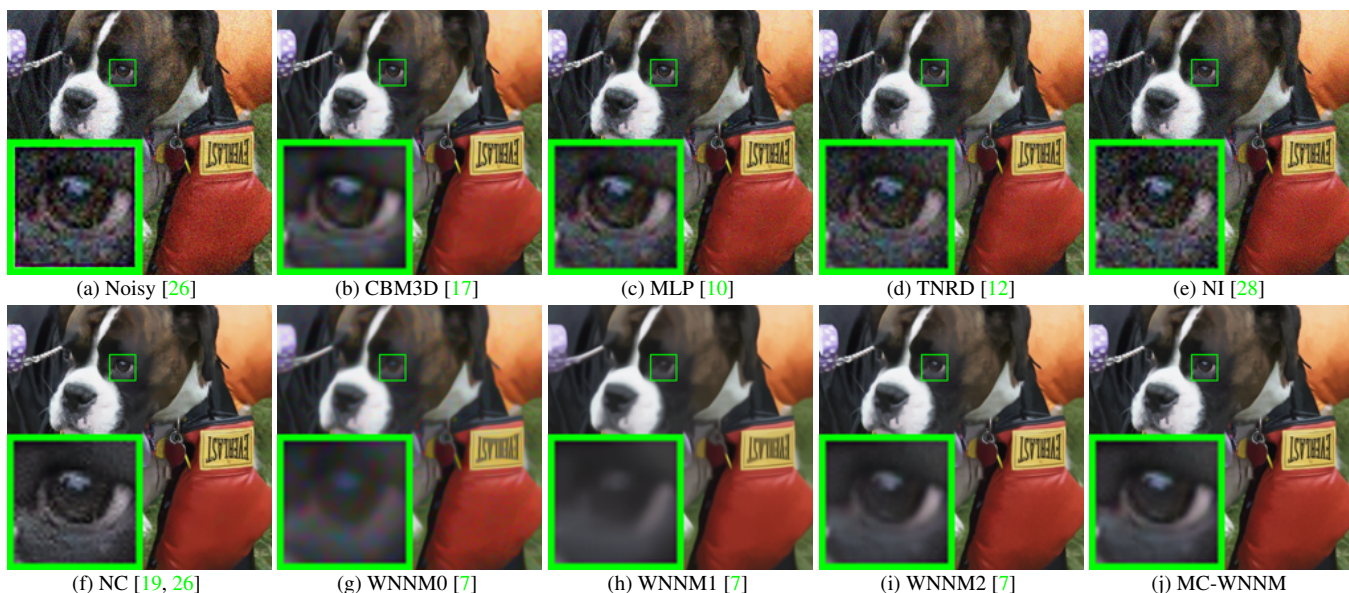
Figure 3. Denoised images of the real noisy image "Dog" [26] by different methods. The images are better to be zoomed in on screen.

"WNNM2", and the proposed MC-WNNM method. The highest PSNR results are highlighted in bold. On average PSNR, the proposed MC-WNNM method achieves 0.44dB improvements over the "WNNM1" method and outperforms the state-of-the-art denoising method CC [14] by 0.83dB. On 10 out of the whole 15 images, the proposed MC-WNNM method achieves the highest PSNR values, while "WNNM1" achieves highest PSNR results on 3 of 15 images. It should be noted that in the CC method, a specific model is trained for each camera and camera setting, while the other methods uses the same model for all

cases. Fig. 4 shows the denoised images of a scene captured by Canon 5D Mark 3 at ISO = 3200. We can see that CBM3D, NI, NC and CC would either remain noise or generate artifacts, while TNRD, "WNNM1", and "WNNM2" over-smooth much the image. Besides, due to treating each channel equally, both the images (g) and (h) in Fig. 4 recovered by "WNNM1" and "WNNM2" have chromatic aberration compared to the mean image (j). The proposed MC-WNNM model achieves better visual quality results than the other methods. More visual comparisons can be found in the supplementary files.

ICCV
#572

ICCV
#572

ICCV 2017 Submission #572. CONFIDENTIAL REVIEW COPY. DO NOT DISTRIBUTE.

Table 2. PSNR(dB) results of different methods on 15 cropped real noisy images used in [14].

Camera Settings		CBM3D	MLP	TNRD	NI	NC	CC	WNNM0	WNNM1	WNNM2	MC-WNNM
Canon 5D Mark III	ISO = 3200	39.76	39.00	39.51	35.68	36.20	38.37	37.51	39.74	39.98	**41.13**
		36.40	36.34	36.47	34.03	34.35	35.37	33.86	35.12	36.65	**37.28**
		36.37	36.33	36.45	32.63	33.10	34.91	31.43	33.14	34.63	**36.52**
Nikon D600	ISO = 3200	34.18	34.70	34.79	31.78	32.28	34.98	33.46	35.08	35.08	**35.53**
		35.07	36.20	36.37	35.16	35.34	35.95	36.09	36.42	36.84	**37.02**
		37.13	39.33	39.49	39.98	40.51	**41.15**	39.86	40.78	39.24	39.56
Nikon D800	ISO = 1600	36.81	37.95	38.11	34.84	35.09	37.99	36.35	38.28	38.61	**39.26**
		37.76	40.23	40.52	38.42	38.65	40.36	39.99	41.24	40.81	**41.43**
		37.51	37.94	38.17	35.79	35.85	38.30	37.15	38.04	38.96	**39.55**
Nikon D800	ISO = 3200	35.05	37.55	37.69	38.36	38.56	39.01	38.60	**39.93**	37.97	38.91
		34.07	35.91	35.90	35.53	35.76	36.75	36.04	37.32	37.30	**37.41**
		34.42	38.15	38.21	40.05	40.59	39.06	39.73	**41.52**	38.68	39.39
Nikon D800	ISO = 6400	31.13	32.69	32.81	34.08	34.25	34.61	33.29	**35.20**	34.57	34.80
		31.22	32.33	32.33	32.13	32.38	33.21	31.16	33.61	33.43	**33.95**
		30.97	32.29	32.29	31.52	31.76	33.22	31.98	33.62	**34.02**	33.94
Average		35.19	36.46	36.61	35.33	35.65	36.88	35.77	37.27	37.12	**37.71**

(a) Noisy kodim07: 37.00dB (b) CBM3D [17]: 39.76dB (c) TNRD [12]: 39.51dB (d) NI [28]: 35.68dB (e) NC [19, 26]: 36.20dB

(f) CC [14]: 38.37dB (g) WNNM1: 39.74dB (h) WNNM2: 39.98dB (i) MC-WNNM: **41.13**dB (j) Mean Image
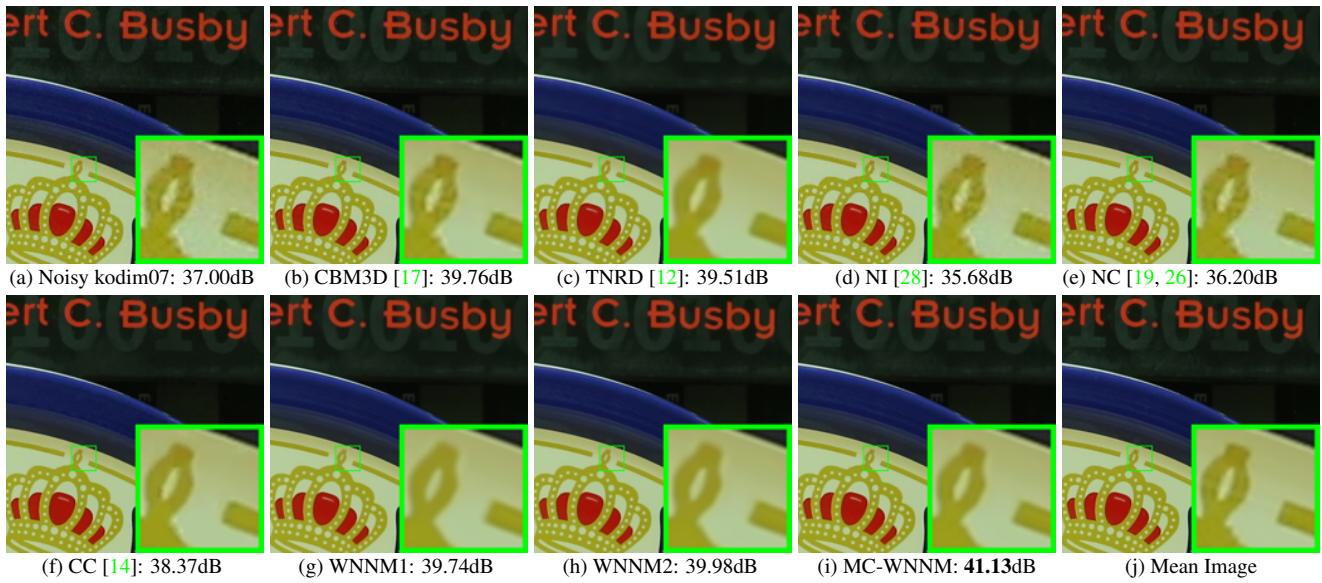
Figure 4. Denoised images of a region cropped from the real noisy image "Canon 5D Mark 3 ISO 3200 1" [14] by different methods. The images are better to be zoomed in on screen.

5. Conclusion and Future Work

The real noisy images have different noise structures among the R, G, B channels due to the preprocessing steps of the digital camera pipelines in CCD or CMOS sensors. This makes the real image denoising problem much more complex than grayscale image denoising. In this paper, we proposed a novel multi-channel (MC) model for real color image denoising. By introducing a weighting matrix to the concatenated weighted nuclear norm minimization (WNNM) model, the proposed MC-WNNM model can process adaptively different noise structures in different channels and exploit the non-local self similarity property of natural images. Though no longer having closed-form solution, the proposed MC-WNNM model is reformulated as a linear equality-constrained problem with two separable variables and successfully solved under the ADMM framework. We also studied the convergence property of the ADMM algorithm. Extensive experiments on synthetic and real color image denoising demonstrate that, the proposed MC-WNNM model outperforms the other competing denoising methods on both synthetic as well as real-world color noisy images. Introducing a weighting matrix to the traditional WNNM model for grayscale image denoising can boost its performance on denoising synthetic and real noisy images. We believe that this work can be extended in at least two directions. Firstly, the weighting matrix beyond the diagonal form, such as correlation form [31], may bring better performance on color image denoising. Secondly, the proposed MC-WNNM model can be extended to deal with hyperspectral images, which may contain hundreds of channels (bands) with different noise structures in different channels.

ICCV
#572

ICCV 2017 Submission #572. CONFIDENTIAL REVIEW COPY. DO NOT DISTRIBUTE.

ICCV
#572

References

[1] A. Buades, B. Coll, and J. M. Morel. A non-local algorithm for image denoising. *IEEE Conference on Computer Vision and Pattern Recognition (CVPR)*, pages 60–65, 2005. 1

[2] K. Dabov, A. Foi, V. Katkovnik, and K. Egiazarian. Image denoising by sparse 3-D transform-domain collaborative filtering. *IEEE Transactions on Image Processing*, 16(8):2080–2095, 2007. 1, 2

[3] M. Elad and M. Aharon. Image denoising via sparse and redundant representations over learned dictionaries. *IEEE Transactions on Image Processing*, 15(12):3736–3745, 2006.

[4] J. Mairal, F. Bach, J. Ponce, G. Sapiro, and A. Zisserman. Non-local sparse models for image restoration. *IEEE International Conference on Computer Vision (ICCV)*, pages 2272–2279, 2009.

[5] W. Dong, L. Zhang, G. Shi, and X. Li. Nonlocally centralized sparse representation for image restoration. *IEEE Transactions on Image Processing*, 22(4):1620–1630, 2013.

[6] J. Xu, L. Zhang, W. Zuo, D. Zhang, and X. Feng. Patch group based nonlocal self-similarity prior learning for image denoising. *IEEE International Conference on Computer Vision (ICCV)*, pages 244–252, 2015.

[7] S. Gu, L. Zhang, W. Zuo, and X. Feng. Weighted nuclear norm minimization with application to image denoising. *IEEE Conference on Computer Vision and Pattern Recognition (CVPR)*, pages 2862–2869, 2014. 1, 2, 5, 7

[8] S. Roth and M. J. Black. Fields of experts. *International Journal of Computer Vision*, 82(2):205–229, 2009. 1

[9] D. Zoran and Y. Weiss. From learning models of natural image patches to whole image restoration. *IEEE International Conference on Computer Vision (ICCV)*, pages 479–486, 2011.

[10] H. C. Burger, C. J. Schuler, and S. Harmeling. Image denoising: Can plain neural networks compete with BM3D? *IEEE Conference on Computer Vision and Pattern Recognition (CVPR)*, pages 2392–2399, 2012. 5, 6, 7

[11] U. Schmidt and S. Roth. Shrinkage fields for effective image restoration. *IEEE Conference on Computer Vision and Pattern Recognition (CVPR)*, pages 2774–2781, June 2014.

[12] Y. Chen, W. Yu, and T. Pock. On learning optimized reaction diffusion processes for effective image restoration. *IEEE Conference on Computer Vision and Pattern Recognition (CVPR)*, pages 5261–5269, 2015. 1, 5, 6, 7, 8

[13] B. Leung, G. Jeon, and E. Dubois. Least-squares luma-chroma demultiplexing algorithm for bayer demosaicking. *IEEE Transactions on Image Processing*, 20(7):1885–1894, 2011. 1, 2

[14] S. Nam, Y. Hwang, Y. Matsushita, and S. J. Kim. A holistic approach to cross-channel image noise modeling and its application to image denoising. *IEEE Conference on Computer Vision and Pattern Recognition (CVPR)*, pages 1683–1691, 2016. 1, 2, 5, 6, 7, 8

[15] H. C. Karaimer and M. S. Brown. A software platform for manipulating the camera imaging pipeline. *European Conference on Computer Vision (ECCV)*, October 2016. 1

[16] Julien Mairal, Michael Elad, and Guillermo Sapiro. Sparse representation for color image restoration. *IEEE Transactions on Image Processing*, 17(1):53–69, 2008. 1, 2

[17] K. Dabov, A. Foi, V. Katkovnik, and K. Egiazarian. Color image denoising via sparse 3D collaborative filtering with grouping constraint in luminance-chrominance space. *IEEE International Conference on Image Processing (ICIP)*, pages 313–316, 2007. 1, 2, 5, 6, 7, 8

[18] C. Liu, R. Szeliski, S. Bing Kang, C. L. Zitnick, and W. T. Freeman. Automatic estimation and removal of noise from a single image. *IEEE Transactions on Pattern Analysis and Machine Intelligence*, 30(2):299–314, 2008. 1, 2

[19] M. Lebrun, M. Colom, and J.-M. Morel. Multiscale image blind denoising. *IEEE Transactions on Image Processing*, 24(10):3149–3161, 2015. 1, 2, 5, 6, 7, 8

[20] F. Zhu, G. Chen, and P.-A. Heng. From noise modeling to blind image denoising. *IEEE Conference on Computer Vision and Pattern Recognition (CVPR)*, June 2016. 1, 2

[21] S. Boyd, N. Parikh, E. Chu, B. Peleato, and J. Eckstein. Distributed optimization and statistical learning via the alternating direction method of multipliers. *Found. Trends Mach. Learn.*, 3(1):1–122, January 2011. 1, 4

[22] C. Lu, C. Zhu, C. Xu, S. Yan, and Z. Lin. Generalized singular value thresholding. *AAAI*, 2015. 1

[23] J. Cai, E. J. Candès, and Z. Shen. A singular value thresholding algorithm for matrix completion. *SIAM Journal on Optimization*, 20(4):1956–1982, 2010. 2

[24] S. Gu, Q. Xie, D. Meng, W. Zuo, X. Feng, and L. Zhang. Weighted nuclear norm minimization and its applications to low level vision. *International Journal of Computer Vision*, pages 1–26, 2016. 2, 3, 4, 5, 6

[25] C. Eckart and G. Young. The approximation of one matrix by another of lower rank. *Psychometrika*, 1(3):211–218, 1936. 2

[26] M. Lebrun, M. Colom, and J. M. Morel. The noise clinic: a blind image denoising algorithm. http://www.ipol.im/pub/art/2015/125/. Accessed 01 28, 2015. 2, 5, 6, 7, 8

[27] C. Kervrann, J. Boulanger, and P. Coupé. Bayesian non-local means filter, image redundancy and adaptive dictionaries for noise removal. *International Conference on Scale Space and Variational Methods in Computer Vision*, pages 520–532, 2007. 2

[28] Neatlab ABSoft. Neat Image. https://ni.neatvideo.com/home. 2, 5, 6, 7, 8

[29] X. Liu, M. Tanaka, and M. Okutomi. Single-image noise level estimation for blind denoising. *IEEE Transactions on Image Processing*, 22(12):5226–5237, 2013. 5

[30] G. Chen, F. Zhu, and A. H. Pheng. An efficient statistical method for image noise level estimation. *IEEE International Conference on Computer Vision (ICCV)*, December 2015. 5, 6

[31] N. J. Higham. Computing the nearest correlation matrix: a problem from finance. *IMA Journal of Numerical Analysis*, 22(3):329, 2002. 8